Twenty-five-fold reduction in measurement uncertainty for a molecular line intensity

Adam J. Fleisher,* Erin M. Adkins, Zachary D. Reed, Hongming Yi, David A. Long, Hélène M. Fleurbaey, and Joseph T. Hodges*

National Institute of Standards and Technology, 100 Bureau Drive, Gaithersburg, MD 20899, USA

Correspondence to: adam.fleisher@nist.gov, joseph.hodges@nist.gov

Dated: 06 June 2019

To accurately attribute sources and sinks of molecules like CO_2, remote sensing missions require line intensities (S) with relative uncertainties $u_r(S)$ < 0.1 %. However, discrepancies in S of ≈1 % are common when comparing different experiments, thus limiting their potential impact. Here we report a cavity ring-down spectroscopy multi-instrument comparison which revealed that the hardware used to digitize analog ring-down signals caused variability in spectral integrals which yield S. Our refined approach improved measurement accuracy twenty-five-fold, resulting in $u_r(S)$ = 0.06 %.

The oscillator strengths of atoms and molecules are, to a high degree of precision, considered invariants of nature and therefore benchmark values for testing fundamental theories of physics and chemistry. The simplest many-body system in nature is the neutral helium atom, whose accurately known oscillator strengths enable validations of various electronic structure theory approximations [1]. Accurate oscillator strengths for molecular hydrogen (and other molecules) are used to model spectra from distant parts of the Universe, and thus constrain variations in the proton-electron mass ratio [2-4], while improved observational and modeling capabilities have leveraged known oscillator strengths to constrain the isotope composition of our solar system [5] and the Universe [6]. More generally, accurate measurements of oscillator strengths for both resonant molecular transitions [7] as well as collision-induced absorption [8] provide important constrains on *ab initio* dipole moment surfaces which predict light-matter interactions for such seemingly intractable extreme environments as exoplanetary atmospheres (e.g., [9]).

Closer to home, remotely located spectrometers designed to answer fundamental questions concerning the Earth's atmosphere also leverage accurately known oscillator strengths (and their derived quantities) to predict light-matter interactions and quantify trends in atmospheric composition. Often, however, independent validation of the dynamic and spatially variable atmospheric samples under study is extremely difficult, if not impossible. In those cases, improved accuracy in the spectroscopic models would reduce or eliminate the need for costly validation experiments.

For example, the high-resolution JAXA Greenhouse Gases Observing Satellite (GOSAT) [10] and NASA Orbiting Carbon Observatory (OCO) [11] passive remote sensing missions have, for more than a decade, relied upon accurate spectroscopic forward models of carbon dioxide (CO_2) and molecular oxygen (O_2) to retrieve CO_2 column densities: the measurement target being a precision of 1 µmol/mol, or approximately 0.3 % of the nominal mean column density [12-14]. Additionally, monitoring global trends in atmospheric methane (CH_4) [15-18] and performing point-source attribution [19] currently motivates laboratory research into accurate first-principles models in congested spectral regions [20, 21], and open-path dual-comb spectroscopy has achieved the following low relative instrumental variations for mole fractions at 30 s of integration: 0.14 % for CO_2, 0.35 % for CH_4, and 0.40 % for water (H_2O) [22]. Consequently, reference values for the absorption cross-sections (derived from the oscillator strengths) of these and many more molecules (e.g., [23]) must be known with sufficiently low relative uncertainty (≤0.1 %) to ensure accurate retrievals from highly precise instruments.

The spectroscopic model for light-matter interactions which relates an observable like spectral transmittance ($\mathcal{T}$) to the mole fraction of absorbing molecules (χ) along a path length (L) is expressed as

$$\chi = -\frac{\ln(\mathcal{T})k_b T}{\sigma p L}, \qquad (1)$$

where k_B is the Boltzmann constant, T is the temperature, p is the pressure, and σ is the absorption cross-section. Assuming that $\mathcal{T}$ is the experimental observable (along with T, p, and L), a suitable model for σ will yield an accurate measurement of χ. At values of T and p routinely encountered within the Earth's atmosphere, σ can comprise a relatively smooth function of frequency, ν, in congested spectral regions (e.g., volatile organic compounds in air [24, 25]), or when the absorber lifetime is short (e.g., collision-induced absorption [8]). When clusters of overlapping lines are resolved (e.g., the overtone spectrum of methane [20, 21]), we can express σ as a summation over a physically justified choice of line shape profiles (including line mixing) scaled by the respective molecular line intensities (S), which can be calculated in terms of invariants of nature. Importantly, this approach yields first-principles models for σ.

In the simplest line-by-line spectral model, σ for small molecules like CO_2 can be expressed as a sum over j well-isolated spectral lines using their known values of S_j and the real-parts of their respective line shape functions, $g_j(\nu)$.

$$\sigma = c \sum_j S_j \, g_j(\nu) + \cdots \qquad (2)$$

In Eq. (2), c is the speed of light and the ellipsis implies additional broadband terms (e.g., spectral baseline). Together, Eqs. (1-2) illustrate a well-known fact: uncertainties in the values of S (and more generally σ) will propagate linearly into uncertainty in atmospheric retrievals of χ (e.g., [12]).

Currently, state-of-the-art *ab initio* calculations of S report relative standard uncertainties, $u_r(S)$, of about 1 %, and preliminary comparisons with the most accurate available experimental data suggests agreement better than 1 % for some rotationally resolved vibrational bands (e.g., [7, 26-29]). However, comparisons between theory and a single optical instrument may be insufficient to capture all type-B (systematic) uncertainty. Unfortunately, line intensities measured across experiments like Fourier-transform spectroscopy (FTS), cavity-enhanced absorption spectroscopy (CEAS), and/or cavity ring-down spectroscopy (CRDS) are known to vary by 1 % to 2 % [29]. Therefore, establishing by consensus the most accurate values and uncertainties for S remains a work in progress [30].

Here we report a multi-instrument comparison between S recorded using three unique CRDS instruments at the National Institute of Standards and Technology (NIST) in Gaithersburg, Maryland. The experiments were performed over a time-period of greater than one year. Our goal was to evaluate the origin and magnitude of the dominant sources of systematic uncertainty in the measurement of S of an individual CO_2 transition, an experimental observable that is proportional to an invariant of nature [29]. We find that, in addition to the standard controls and measures of sample temperature, pressure, optical frequency, line shape profile, and certified absorber mole fraction, a quantitative evaluation of previously uncharacterized CRDS signal digitizer nonidealities was required to reduce $u_r(S)$ to our minimum achieved value of $u_r(S)$ = 0.06 %. By calibrating numerous CRDS digitizers using a metrology-grade reference digitizer with high static linearity and synthetic exponential decay signals (SEDS), we achieved a twenty-five-fold reduction in $u_r(S)$ relative to the current literature value of $u_{lit}(S)$ = 1-2 % [29]. Using this approach, we met the longstanding goal of quantifying S with sufficient precision and accuracy needed in first-principles calculations of absorption cross-sections for the most ambitious optical remote sensing missions. Moreover, we achieved this goal for the CO_2 transition under consideration for active remote sensing by the NASA Active Sensing of CO_2 Emissions over Nights, Days, and Seasons (ASCENDS) mission [31].

In an idealized CRDS experiment performed with a single-frequency continuous-wave laser, the passive decay of optical power from a high-finesse optical resonator is purely exponential, and the cavity time constant (τ) encodes the round-trip intracavity losses (e.g., molecular absorption). Generally, optical decays are converted to analog electrical signals by a photoreceiver and then digitized by an analog-to-digital converter (ADC) for software analysis. Deviations from purely exponential behavior arising from common sources like photoreceiver saturation, incomplete laser shuttering, or interfering optical resonator modes are readily identified by systematic residuals in the fitted decays. However, slight nonidealities in the digitizer hardware are not so readily identified and could be particularly problematic for nonlinear CRDS methods [32]. To date, only large digitizer nonidealities have been discussed in the CRDS literature [33]. Here we hypothesize that each of our common digitizers has a unique power law

response that governs its static linearity, and that slight deviations from a unity exponent in that power law systematically alter the observed values of τ without introducing nonexponential time dependence of the digitized electronic signals.

A general illustration of the CRDS approach is shown in Fig. 1. While each of the three spectrometers used here were unique, they shared several common properties. The central component of each instrument was a high-finesse, linear two-mirror optical resonator which contained a flowing gas sample (actual mass flow rates of 0.02-0.04 L/min) of NIST Standard Reference Material (SRM) gas mixture 1721-A-29, Southern Oceanic Air, with a certified CO_2 mole fraction of χ_{CO_2} = (387.98 ± 0.05) µmol/mol ($u_r(\chi_{CO_2})$ = 0.013 %) [34, 35]. For each instrument, a continuous-wave laser was spatially mode-matched and injected into the stable optical resonator to interrogate CO_2 absorption, specifically the R 16e $^{12}C^{16}O_2$ rotational transition within the 30012 – 00001 vibrational band (center wave number of $\tilde{\nu}_0$ = 6359.967 cm^{-1} [29]). Following optical buildup to a predetermined transmission threshold, the probe laser was optically shuttered and passive cavity decays were observed on a photoreceiver, digitized, and fitted in real time with an exponential decay to provide the τ as a function of laser frequency.

All three CRDS instruments utilized here were previously reported in part. Spectrometer 1 (S1) was a frequency-stabilized (FS) CRDS [36] instrument with a nominal cavity length L = 139 cm, single-pass base losses ℓ = 3.3 × 10^{-5}, laser line width of δ ≈ 100 kHz, photoreceiver minimum noise-equivalent power of NEP = 0.34 pw $Hz^{-1/2}$ and an electronic bandwidth of B = 8 MHz, and optical trigger threshold of V_{Trig} = 1 V [37]. Spectrometer 2 (S2) was also an FS-CRDS instrument, but with nominal L = 75 cm, ℓ = 1.68 × 10^{-4}, δ ≈ 300 kHz, NEP = 0.34 pw $Hz^{-1/2}$ and B = 6 MHz, and V_{Trig} = 2.5 V [26]. Spectrometer 3 (S3) was a frequency-agile, rapid scanning (FARS) CRDS [38] instrument with nominal L = 74 cm, ℓ = 3.0 × 10^{-5}, δ ≈ 130 Hz, NEP = 0.34 pw $Hz^{-1/2}$ and B = 300 kHz, and V_{Trig} = 2 V [39]. As a result of their design, the spectrometer empty-cavity time constants spanned one order-of-magnitude (from 14.9 µs for S2 to 142 µs for S1), thus providing substantially different working parameters over which to evaluate digitizer biases. The considerable differences in number and identity of optical components and their alignment also aided to randomize baseline effects (e.g., etalons) between spectrometers, and variations in spectral sampling density and spectral window also served to randomize differences between the measurements.

To test for variations in digitizer nonidealities, cavity decays from each spectrometer S1-S3 were digitized by either the reference digitizer, one of several calibrated digitizers, or both. The reference digitizer (National Instruments PCI-5922 [40]) was a highly linear digitizer that has found application in alternating-current (AC) electrical metrology [41-42]. As such, the reference digitizer (hereafter also referred to as D1) was used as a transfer standard to compare the performance of other digitizers (D2-D5), which while common in CRDS, have not been adequately characterized for their conversion fidelity. A summary of our independent evaluation of D1's static linearity (DC to 10 kHz) is available in the Supplemental Material [43].

In brief, the calibrated digitizers D2-D5 were each a direct-current (DC) coupled, full-sized peripheral-component interconnect express (PCIe) digitizer board with sampling rate F_s = 200 MS/s, digitization bandwidth B = 125 MHz, vertical range V_{pp} = ± 10 V, and vertical resolution Δ = 16 bits. The calibrated digitizers D2-D5 were evaluated with respect to the reference digitizer D1 using SEDS from an arbitrary waveform generator (Agilent M8190A [40] operating at F_s = 128 MS/s). The SEDS acted as a proxy for a full DC-AC analysis [41-43] and enabled a direct evaluation of D2-D5 performance for CRDS. When necessary to reproduce experimental conditions, SEDS were amplified and offset prior to evaluation by

the reference digitizer using linear analog electronics including amplifiers, DC voltage sources, and/or a summing amplifier with 1 MHz of electronic bandwidth and total harmonic distortion of ≤ 10^{-4} at 1 kHz (Stanford Research Systems Small Instrument Modules [40]). The SEDS time constants measured by the reference digitizer D1 (τ_{SEDS}) were used to calibrate the apparent time constants (τ_A) measured by digitizers D2-D5. The resulting D2-D5 calibration coefficients b_1 and b_0 from the fitted equation $\tau_{SEDS} = b_1\tau_A + b_0$ are listed in the Supplemental Material [43], along with the empty-cavity τ (τ_0) measured for spectrometers S1-S3. Digitizers were interchanged in some instances, resulting in the following six unique combinations of digitizer and spectrometer: D1-S1, D1-S3, D2-S3, D3-S1, D4-S2 and D5-S2. We therefore report a comparison across six values of S for the R 16e transition within the 30012 – 00001 band of $^{12}C^{16}O_2$.

The b_1 and b_0 digitizer calibration coefficients were used to calculate cavity time constants (τ) from the measured τ_A by the equation $\tau = b_1\tau_A + b_0$, and therefore resulted in absorption spectra of CO_2 that were corrected for bias introduced by the digitizers. The empirical procedure outlined above ensured that all values of τ measured by each unique digitizer-spectrometer combination were linked to the metrology-grade reference digitizer D1 with high static linearity [41-43]. Note that the empirical D2-D5 calibration procedure accounted for all sources of electronic distortion and/or bias from the photoreceiver output to the digitizer input, as well as biases inherent to D2-D5. For all cases, the b_1 and b_0 coefficients were determined by replacing the spectrometer photoreceiver output with the SEDS, thus evaluating the entire electronic chain for each respective S1-S3 instruments preceding D2-D5. The electronic chain preceding each digitizer was unique for each spectrometer, and, for example, included various electronic cables and splitters, delay generators, filters, and/or additional digitizers and oscilloscopes which could result in unwanted back reflections, impedance mismatches, thermo-electric voltages from dissimilar connector metals, and various types of AC pickup and interference. When using the reference digitizer D1 to measure S_{int} (D1-S1 and D1-S3), no calibrations were performed, and all efforts were made to minimize biases associated with the up-stream electrical chain.

Representative unbiased and apparent spectra of the R 16e transition within the 30012 – 00001 $^{12}C^{16}O_2$ band recorded using the D4-S2 combination and a sample pressure of 8.88 kPa are plotted in Fig. 2. Shown in blue open circles are the apparent loss-per-unit length (sample absorption coefficient plus base losses equal to $\alpha_A(\nu) = 1/c\tau_A(\nu)$ in units of cm^{-1}. The unbiased values ($\alpha(\nu) = 1/c\tau(\nu)$) are shown as solid red squares, along with the corresponding fitted model (red line). The fitted residuals are also plotted as a red line in the middle panel. In the bottom panel of Fig. 2, the relative difference between the apparent and unbiased absorption coefficients ($\alpha_A/\alpha - 1 = \tau/\tau_A - 1$) is plotted as black dots. To model the experimental line shape profiles, we used the speed-dependent Nelkin-Ghatak profile (SDNGP), a limiting case of the Hartmann-Tran profile (HTP) [44]. The spectral model for fitting was completed by including a linear baseline function and, when necessary, sine functions to model undesired optical etalons.

For each digitizer-spectrometer combination, line areas $A = \int \alpha(\nu)d\nu$ were measured at a minimum of four pressures over the range of 8.7 kPa to 27 kPa (65 Torr to 200 Torr). Linear fits of A vs. absorber number density ($\rho = p/k_BT$) yielded S for the R 16e CO_2 transition (corrected to T = 296 K using the known CO_2 total partition function and lower state energy [29, 45]). The individual S values are tabulated in the Supplemental Material [43], along with the apparent values (S_A) extracted from linear fits of the apparent line areas $A_A = \int \alpha_A(\nu)d\nu$ versus ρ, the relative changes in S_A following calibration, and the individual relative standard uncertainties $u_{i,r}(S)$. Even at the highest pressure of 27 kPa, we

observe no evidence of significant collisional effects beyond the impact approximation like those investigated for polar molecules like HF and HCl and in high-pressure (p > 200 kPa) buffer gases of Xe and Ar, respectively [46, 47]. No systematic deviations in the residuals of the linear fits of A vs. ρ were observed. Because the buffer-gas effects (e.g., dimerization, etc.) decrease rapidly with increasing rotational quantum number J, we anticipate little effect on the retrieved values of S at T = 296 K for the J = 16 transition of CO_2.

Plotted respectively in Fig. 3 are the unbiased S (blue circles) and apparent S_A (orange squares) values for each digitizer-spectrometer combination relative to the weighted mean value of $\langle S \rangle$ = (1.7589 ± 0.0011) × 10^{-23} cm/molecule, where the weighting factors for calculating $\langle S \rangle$ were $w_i = u_i^{-2}$. Although the $u_i(S)$ values comprised both type-A and type-B uncertainties [43], we assumed that the individual type-B (systematic) uncertainties attributed to each unique digitizer-spectrometer combination were uncorrelated with respect to the other combinations. For example, the individual type-B uncertainties related to sample temperature (T) were considered uncorrelated because each spectrometer utilized a different temperature probe and mounting configuration. Assuming $u_i(S)$ were uncorrelated, we estimated the type-A uncertainty in our final value of S to equal the standard error of the weighted mean of all six digitizer-spectrometer combinations ($u_{r,\mathrm{A}}(S)$ = 0.059 %). In addition to $u_{r,\mathrm{A}}(S)$, the combined relative uncertainty budget for S also included two type-B uncertainties common to all digitizer-spectrometer combinations: uncertainty in the sample mole fraction of 0.013 % and uncertainty in our evaluation of the static linearity of the reference digitizer D1 of 0.002 % [43]. A quadrature sum of uncertainties yielded the reported relative standard uncertainty of $u_r(S)$ = 0.06 %, dominated by $u_{r,\mathrm{A}}(S)$. The reported value of $u_r(S)$ = 0.06 % is a more than six-fold reduction in uncertainty as compared to that calculated from values of S_A (0.4 %), and a more than twenty-five-fold improvement as compared to the literature ($u_{lit}(S) \approx 2$ %) [29].

Figure 3 shows that we identified and corrected (orange boxes) a previously uncharacterized source of significant systematic (type-B) uncertainty in high-precision CRDS: digitization nonidealities. Using an empirical calibration procedure and a metrology-grade reference digitizer, the newly considered digitizer bias was largely removed, and independent measurements of a molecular line intensity converged to within the measurement precision. By comparison across multiple unique CRDS instruments, we randomized any remaining type-B uncertainties inherent to our spectroscopic approach or individual instrumentation and significantly reduced the relative combined uncertainty to below the 10^{-3} level. In the future, additional independent measurements will therefore provide further statistical reduction in uncertainty. Furthermore, comparisons between various types of cavity-enhanced spectroscopies [48] would provide valuable independent checks of our CRDS-based measurement approach.

The digitizer bias correction procedure presented here, with traceability to an electrical metrology-grade reference digitizer [41, 42], is applicable to stand-alone instruments and could be used to generally confirm or improve the accuracy of measured cavity ring-down spectroscopy decay times. The realization of accurate and precise measurements of line intensities below the 10^{-3} level opens the possibility of pushing against other measurement boundaries related to sample conditions (e.g., temperature, pressure, absorber mole fraction, etc.). Ultimately, referencing digitizer static linearity at both V_{DC} and V_{AC} to traceable electrical metrology tools linked to the new international system of units [49, 50], or quantum-SI, could enable accuracy and SI-traceability for direct absorption spectroscopy below the 10^{-4} level.

Acknowledgements

We acknowledge Jason Underwood and Stefan Cular (NIST) for discussions regarding electrical metrology and digitizer characterization and Christopher W. Meyer (NIST) for a multimeter instrument loan. We also acknowledge funding from the NIST Greenhouse Gas and Climate Science Program and from NASA Spectroscopy in Support of the OCO Missions.

References

1. J. Li, M. Holzmann, I. Duchemin, X. Blase and V. Olevano, "Helium atom excitations by the *GW* and Bethe-Salpeter many-body formalism," *Phys. Rev. Lett.* **118,** 163001 (2017).
2. J. Bagdonaite, W. Ubachs, M. T. Murphy and J. B. Whitmore, "Constraint on a varying proton-electron mass ratio 1.5 billion years after the big band," *Phys. Rev. Lett.* **114,** 071301 (2015).
3. W. Ubachs, J. C. J. Koelemeij, K. S. E. Eikema, E. J. Salumbides, "Physics beyond the Standard Model from hydrogen spectroscopy," *J. Mol. Spectrosc.* **320,** 1-12 (2016).
4. W. Ubachs, "Search for varying constants of nature from astronomical observations of molecules," *Space Sci. Rev.* **214,** 3 (2018).
5. P. R. Mahaffy, C. R. Webster, S. K. Atreya, H. Franz, M. Wong, P. G. Conrad, D. Harpold, J. J. Jones, L. A. Leshin, MSL Science Team, "Abundance and isotopic composition of gases in the Martian atmosphere from the Curiosity Rover," *Science* **341,** 263-266 (2013).
6. K. Lind, J. Melendez, M. Asplund, R. Collet and Z. Magic, "The lithium isotopic ratio in very metal-poor stars," *Astron. Astrophys.* **554,** A96 (2013).
7. O. L. Polyansky, K. Bielska, M. Ghysels, L. Lodi, N. F. Zobov, J. T. Hodges and J. Tennyson, "High-accuracy CO_2 line intensities determined from theory and experiment," *Phys. Rev. Lett.* **114,** 243001 (2015).
8. T. Karman, M. A. J. Koenis, A. Banerjee, D. H. Parker, I. E. Gordon, A. van der Avoird, W. J. van der Zande and G. C. Groenenboom, "O_2-O_2 and O_2-N_2 collision-induced absorption mechanisms unraveled," *Nat. Chemistry* **10,** 549-554 (2018).
9. J. Tennyson, S. N. Yurchenko, A. F. Al-Refaie, E. J. Barton, K. L. Chubb, P. A. Coles, S. Diamantopoulou, M. N. Gorman, C. Hill, A. Z. Lam, et al., "The ExoMol database: molecular line lists for exoplanet and other hot atmospheres," *J. Mol. Spectrosc.* **327,** 73-94 (2016).
10. A. Kuze, H. Suto, M. Nakajima and T. Hamazaki, "Thermal and near infrared sensor for carbon observation Fourier-transform spectrometer on the Greenhouse Gases Observing Satellite for greenhouse gases monitoring," *Appl. Opt.* **48,** 6716-6733 (2009).
11. D. Crisp, R. M. Atlas, F.-M. Breon, L. R. Brown, J. P. Burrows, P. Ciais, B. J. Conner, S. C. Doney, I. Y. Fung, D. J. Jacob, et al., "The Orbiting Carbon Observatory (OCO) mission," *Adv. in Space Res.* **34,** 700-709 (2004).
12. C. E. Miller, L. R. Brown, R. A. Toth, D. C. Benner and V. M. Devi, "Spectroscopic challenges for high accuracy retrievals of atmospheric CO_2 and the Orbiting Carbon Observatory (OCO) experiment," *C. R. Physique* **6,** 876-887 (2005).
13. F. M. Schwandner, M. R. Gunson, C. E. Miller, S. A. Carn, A. Eldering, T. Krings, K. R. Verhulst, D. S. Schimel, H. M. Nguyen, D. Crisp, et al., "Spaceborne detection of localized carbon dioxide sources," *Science* **358,** eaam5782 (2017).
14. P. Bergamaschi, C. Frankenberg, J. F. Meirink, M. Krol, M. G. Villani, S. Houweling, F. Dentener, E. J. Dlugokencky, J. B. Miller, L. V. Gatti, et al., "Inverse modeling of global and regional CH_4 emissions using SCIAMACHY satellite retrievals," *J. Geophys. Res. Atmos.* **114,** D22301 (2009).
15. R. Parker, H. Boesch, A. Cogan, A. Fraser, L. Feng, P. I. Palmer, J. Messerschmidt, N. Deutscher, D. W. T. Griffith, J. Notholt, et al., "Methane observations from the Greenhouse Gases Observing SATellite: Comparison to ground-based TCCON data and model calculations," *Geophys. Res. Lett.* **38,** L15807 (2011).

16. C. Stephan, M. Alpers, B. Millet, G. Ehret, P. Flamant, C. Deniel, "MERLIN: a space-based methane monitor," Proc. SPIE 8159, Lidar Remote Sensing for Environmental Monitoring XII, 815908 (13 September 2011).
17. H. Riris, K. Numata, S. Li, S. Wu, A. Ramanathan, M. Dawsey, J. Mao, R. Kawa and J. B. Abshire, "Airborne measurements of atmospheric methane column abundance using a pulsed integrated-path differential absorption lidar," *Appl. Opt.* **51,** 8296-8305 (2012).
18. J. Tollefson, "Big prize for methane probe," *Nature* **556,** 283 (2018).
19. S. Coburn, C. B. Alden, R. Wright, K. Cossel, E. Baumann, G.-W. Truong, F. Giorgetta, C. Sweeney, N. R. Newbury, K. Prasad, et al. "Regional trace-gas source attribution using a field-deployable dual frequency comb spectrometer," *Optica* **5,** 320-327 (2018).
20. T. Delahaye, S. E. Maxwell, Z. D. Reed, H. Lin, J. T. Hodges, K. Sung, V. M. Devi, T. Warneke, P. Spietz and H. Tran, "Precision methane absorption measurements in the 1.64 µm spectral region for the MERLIN mission," *J. Geophys. Res. Atmos.* **121,** 7360-7370 (2016).
21. T. Delahaye, M. Ghysels, J. T. Hodges, K. Sung, R. Armante and H. Tran, "Measurement and modeling of air-broadened methane absorption in the MERLIN spectral region at low temperatures," *J. Geophys. Res. Atmos.* **124,** 3556-3564 (2019).
22. E. M. Waxman, K. C. Cossel, G.-W. Truong, F. R. Giorgetta, W. C. Swann, S. Coburn, R. J. Wright, G. B. Rieker, I. Coddington and N. R. Newbury, "Intercomparison of open-path trace gas measurements with two dual-frequency-comb spectrometers," *Atmos. Meas. Tech.* **10,** 3295-3311 (2017).
23. P. F. Bernath, "The Atmospheric Chemistry Experiment (ACE)," *J. Quant. Spectrosc. Radiat. Transfer* **186,** 3-16 (2017).
24. G. Ycas, F. R. Giorgetta, E. Baumann, I. Coddington, D. Herman, S. A. Diddams and N. R. Newbury, "High-coherence mid-infrared dual-comb spectroscopy," *Nat. Photonics* **12,** 202-208 (2018).
25. G. Ycas, F. R. Giorgetta, K. C. Cossel, E. M. Waxman, E. Baumann, N. R. Newbury and I. Coddington, *Optica* **6,** 165-168 (2019).
26. H. Yi, Q. Liu, A. J. Fleisher and J. T. Hodges, "High-accuracy $^{12}C^{16}O_2$ line intensities in the 2 µm wavelength region measured by frequency-stabilized cavity ring-down spectroscopy," *J. Quant. Spectrosc. Radiat. Transfer* **206,** 367-377 (2017).
27. P. Guay, J. Genest and A. J. Fleisher, "Precision spectroscopy of $H^{13}CN$ using a free-running, all-fiber dual electro-optic frequency comb system," *Opt. Lett.* **43,** 1407-1410 (2018).
28. V. Yu. Makhnev, A. A. Kyuberis, O. L. Polyansky, I. I. Mizus, J. Tennyson and N. F. Zobov, "A new spectroscopically-determined potential energy surface and *ab initio* dipole moment surface for high accuracy HCN intensity calculations," *J. Mol. Spectrosc.* **353,** 40-53 (2018).
29. I. E. Gordon, L. S. Rothman, C. Hill, R. V. Kochanov, Y. Tan, P. F. Bernath, M. Birk, V. Boudon, A. Campargue, K. V. Chance, et al., "The HITRAN2016 molecular spectroscopic database," *J. Quant. Spectrosc. Radiat. Transfer* **203,** 3-69 (2017).
30. F. Oyafuso, V. H. Payne, B. J. Drouin, V. M. Devi, D. C. Benner, K. Sung, S. Yu, I. E. Gordon, R. Kochanov, Y. Tan, et al., "High accuracy absorption coefficients for the Orbiting Carbon Observatory-2 (OCO-2) mission: Validation of updated carbon dioxide cross-sections using atmospheric spectra," *J. Quant. Spectrosc. Radiat. Transfer* **203,** 213-223 (2017).
31. S. R. Kawa, J. Mao, J. B. Abshire, G. J. Collatz, X. Sun and C. J. Weaver, "Simulation studies for a space-based CO_2 lidar mission," *Tellus B* **62,** 759-769 (2010).
32. G. Giusfredi, S. Bartalini, S. Borri, P. Cancio, I. Galli, D. Mazzotti and P. De Natale, "Saturated-absorption cavity ring-down spectroscopy," *Phys. Rev. Lett.* **104,** 110801 (2010).

33. S. Wójtewicz, D. Lisak, A. Cygan, J. Domysławska, R. S. Trawiński and R. Ciuryło, "Line-shape study of self-broadened O_2 transitions measured by Pound-Drever-Hall-locked frequency-stabilized cavity ring-down spectroscopy," *Phys. Rev. A* **84,** 032511 (2011).
34. G. C. Rhoderick, M. E. Kelley, W. R. Miller, G. Brailsford and A. Possolo, "Development of a southern oceanic air standard reference material," *Anal. Bioanal. Chem.* **408,** 1159-1169 (2016).
35. Assuming $\delta\ ^{13}C$ = −8.3 ‰ and $\delta\ ^{18}O$ = 1.0 ‰ (Vienna Pee Dee Belemnite CO_2 scale) for the SRM gas sample reported in [34], we estimated the mole fraction of $^{12}C^{16}O_2$ to be χ_{626} = 0.98412447 × χ_{CO_2}. Note that the accurate value of S reported herein was scaled to χ_{626} = 0.984204 adopted by HITRAN2016 [27]; a relative adjustment of only 0.008 %.
36. J. T. Hodges, H. P. Layer, W. W. Miller and G. E. Scace, "Frequency-stabilized single-mode cavity ring-down apparatus for high-resolution absorption spectroscopy," *Rev. Sci. Instrum.* **75,** 849-863 (2004).
37. H. Lin, Z. D. Reed, V. T. Sironneau and J. T. Hodges, "Cavity ring-down spectrometer for high-fidelity molecular absorption measurements," *J. Quant. Spectrosc. Radiat. Transfer* **161,** 11-20 (2015).
38. G.-W. Truong, K. O. Douglass, S. E. Maxwell, R. D. van Zee, D. F. Plusquellic, J. T. Hodges and D. A. Long, "Frequency-agile, rapid scanning spectroscopy," *Nat. Photonics* **7,** 532-534 (2013).
39. D. A. Long, S. Wójtewicz, C. E. Miller and J. T. Hodges, "Frequency-agile, rapid scanning cavity ring-down spectroscopy (FARS-CRDS) measurements of the (30012)←(00001) near-infrared carbon dioxide band," *J. Quant. Spectrosc. Radiat. Transfer* **161,** 35-40 (2015).
40. Certain commercial equipment is identified in this paper in order to specify the experimental procedure adequately. Such identification is not intended to imply recommendation or endorsement by the National Institute of Standards and Technology, nor is it intended to imply that the equipment identified is necessarily the best available for the purpose.
41. F. Overney, A. Rüfenacht, J.-P. Braun, B. Jeanneret and P. S. Wright, "Characterization of metrological grade analog-to-digital converters using a programmable Josephson voltage standard" *IEEE Trans. Instrum. Meas.* **60,** 2172-2177 (2011).
42. G. Rietveld, D. Zhao, C. Kramer, E. Houtzager, O. Kristensen, C. de Leffe and T. Lippert, "Characterization of a wideband digitizer for power measurements up to 1 MHz," *IEEE Trans. Instrum. Meas.* **60,** 2195-2201 (2011).
43. See Supplemental Material at **[URL will be inserted by publisher]** for a summary of the reference digitizer D1 comparisons with the high-precision multimeter, as well as the individual digitizer-spectrometer data including calibration coefficients (b_1, b_0), empty-cavity time constants (τ_0), measured apparent (S_A) and unbiased (S) line intensities, the relative changes in line intensities, relative combined uncertainties (u_r), and a representative uncertainty budget.
44. J. Tennyson, P. F. Bernath, A. Campargue, A. G. Császár, L. Daumont, R. R. Gamache, J. T. Hodges, D. Lisak, O. V. Naumenko, L. S. Rothman, et al., "Recommended isolated-line profile for representing high-resolution spectroscopic transitions (IUPAC Technical Report)," *Pure Appl. Chem.* **86,** 1931-1943 (2014).
45. R. R. Gamache, C. Roller, E. Lopes, I. E. Gordon, L. S. Rothman, O. L. Polyansky, N. F. Zobov, A. A. Kyuberis, J. Tennyson, S. N. Yurchenko, et al., "Total internal partition sums for 166 isotopologues of 51 molecules important in planetary atmospheres: Application to HITRAN2016 and beyond," *J. Quant. Spectrosc. Radiat. Transfer* **203,** 70-87 (2017).
46. A. P. Kouzov, K. G. Tokhadze and S. S. Utkina, "Buffer-gas effects on the rotovibrational line intensity distribution: analysis of possible mechanisms," *Eur. Phys. J. D* **12,** 153-159 (2000).

47. C. Boulet, P.-M. Flaud and J.-M. Hartmann, “Infrared line collisional parameters of HCl in argon, beyond the impact approximation: measurements and classical path calculations,” *J. Chem. Phys.* **120,** 11053-11061 (2004).
48. A. Cygan, S. Wójtewicz, G. Kowzan, M. Zaborowski, P. Wcisło, J. Nawrocki, P. Krehlik, Ł. Śliwczyński, M. Lipiński, P. Masłowski, et al. “Absolute molecular transition frequencies measured by three cavity-enhanced spectroscopy techniques,” *J. Chem. Phys.* **144,** 214202 (2016).
49. C. J. Burroughs, Jr., P. D. Dresselhaus, A. Rüfenacht, D. Olaya, M. M. Elsbury, Y.-H. Tang and S. P. Benz, “NIST 10 V programmable Josephson voltage standard system,” *IEEE Trans. Instrum. Meas.* **60,** 2482-2488 (2011).
50. N. E. Flowers-Jacobs, A. E. Fox, P. D. Dresselhaus, R. E. Schwall and S. P. Benz, “Two-volt Josephson arbitrary waveform synthesizer using Wilkinson dividers,” *IEEE Trans. Appl. Supercond.* **26,** 1400207 (2016).

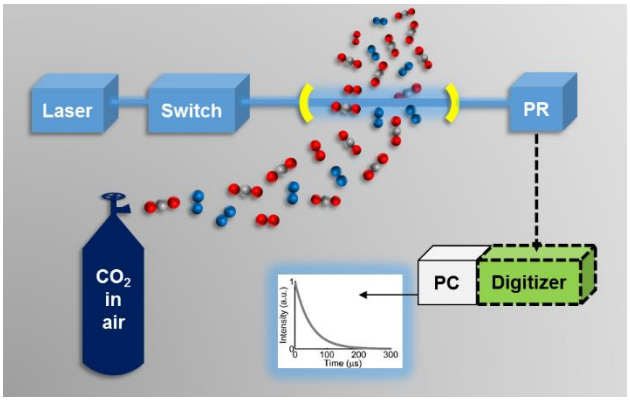

Fig. 1. General illustration of a cavity ring-down spectrometer. From the top left, a continuous-wave laser (blue lines) was injected into an optical cavity (yellow curved mirrors) containing a flowing gas sample of CO_2-in-air (gray: carbon, red: oxygen, blue: nitrogen). Upon reaching a predefined transmission threshold, an optical switch shuttered the laser and passive cavity decays were observed incident on a photoreceiver (PR). The electrical output of the PR (black dashed arrow) was coupled to an analog-to-digital converter (ADC, or digitizer), and the resulting digitized decay signals were fitted in real time using home-built acquisition software and a personal computer (PC).

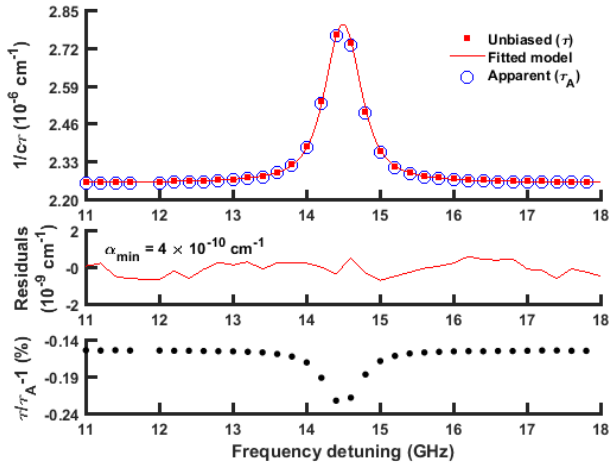

Fig. 2. A portion of representative unbiased (red squares) and apparent (blue circles) spectra of the R 16e CO_2 transition with $\tilde{\nu}_0$ = 6359.967 cm^{-1} are shown in the top panel. Fitted spectra spanned a frequency detuning range of 0 GHz to 28 GHz, the sample pressure was 8.88 kPa, and the sample CO_2 mole fraction was χ_{CO_2} = (387.98 ± 0.05) µmol/mol. The apparent spectrum was recorded by the digitizer-spectrometer combination D4-S2, and τ_A were corrected to yield τ using the coefficients in the Supplemental Material [43]. A fitted model of the unbiased absorption coefficient ($\alpha = 1/c\tau$) is also shown as a red line and fitted residuals are plotted as another red line in the middle panel. In the bottom panel, the relative difference $\tau/\tau_A - 1$ (equal to $\alpha_A/\alpha - 1$, where α_A is the apparent absorption coefficient) is plotted as black dots.

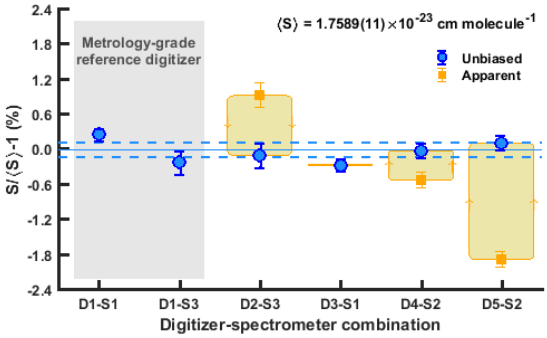

Fig. 3. Unbiased (S, blue circles) and apparent (S_A, orange squares) values of the R 16e CO_2 line intensity at T = 296 K (30012 – 00001 band). Error bars show ±1σ standard uncertainties. The gray shaded region comprising D1-S1 and D1-S3 (far left) highlights values of S measured by the metrology-grade reference digitizer. For values of S with corresponding values of S_A, light orange boxes indicate the magnitude of each digitizer correction. The light blue dashed lines bound the standard deviation of the weighted mean value of $\langle S \rangle$ (solid blue line).